The WISDOM radar on board the ExoMars 2022 Rover: Characterization and calibration of the flight model

Yann Herve, Valérie Ciarletti, Alice Le Gall, Charlotte Corbel, Rafik Hassen-Khodja, W. S. Benedix, D. Plettemeier, Olivier Humeau, André-Jean Vieau, Benjamin Lustrement, et al.

Planetary and Space Science 189 (2020) 104939

Contents lists available at ScienceDirect

Planetary and Space Science

journal homepage: www.elsevier.com/locate/pss

The WISDOM radar on board the ExoMars 2022 Rover: Characterization and calibration of the flight model

Y. Hervé [a,*], V. Ciarletti [a], A. Le Gall [a,b], C. Corbel [a], R. Hassen-Khodja [a], W.S. Benedix [c], D. Plettemeier [c], O. Humeau [a], A.J. Vieau [a], B. Lustrement [a], S. Abbaki [a], E. Bertran [a], L. Lapauw [a], V. Tranier [a], N. Oudart [a], F. Vivat [a], C. Statz [c], Y. Lu [c], S. Hegler [c], A. Hérique [d]

[a] LATMOS/IPSL, UVSQ Université Paris-Saclay, Sorbonne Université, CNRS, Paris, France
[b] Institut Universitaire de France (IUF), Paris, France
[c] Technische Universität Dresden, Dresden, Germany
[d] Univ. Grenoble Alpes, CNRS, IPAG, Grenoble, France

ARTICLE INFO

Keywords:
Mars
ExoMars
Subsurface
WISDOM
Ground penetrating radar
Calibration

ABSTRACT

The ground penetrating radar WISDOM on board the Rover of the ExoMars 2022 mission (ESA/Roscosmos) will be a pioneer in the exploration of the Martian subsurface from the surface (until now, Martian sounding radars have been operated from orbit). WISDOM will image the first meters below the surface of Oxia Planum — the ExoMars 2022 landing site — with the objectives of revealing its geological history and identifying safe and promising scientific targets for subsurface sampling by the Rover drill. In this paper, we present the qualification, characterization and calibration tests that have been conducted on WISDOM flight model in order to assess its performance, build the data processing pipeline and prepare scientific return of this experiment. In most favorable but geologically plausible cases (low loss and homogeneous subsurface, smooth interface), WISDOM can detect a buried interface down to a depth of 8 m with a vertical resolution of 3 cm (for a subsurface dielectric constant of 4). Its penetration depth is typically 2 m in less favorable environments. For safety reason, WISDOM antennas are accommodated 38 cm above the ground; the amplitude of the surface echo will be used to estimate the top layer dielectric constant with an accuracy of 13% which translates into an accuracy of 6% on the distance/depth assessment. WISDOM data processing chain includes corrections aiming at removing parasitic signals of various origins (electronic coupling, antenna crosstalk, multiple surface echoes, etc.) and at correcting the data to a reference temperature and antenna elevation; it has been designed to automatically produce calibrated radargrams in less than 20 min as required for the mission operations. Additional more sophisticated processing will be manually run in parallel. The impact of the Rover structure on measurements has been investigated and can be partially removed.

1. Introduction

In March 2021, the ESA (European Space Agency)-Roscosmos ExoMars Rover and surface science platform will land on Mars, at Oxia Planum (Quantin-Nataf et al., 2019a, 2019b; Ciarletti et al., 2015). The Rover will explore this ancient water-rich environment on the quest to discover traces of life (Vago et al., 2017). As a consequence of the destructive effects of ionizing radiation and atmospheric oxidants, the surface of Mars is today a hostile place for life. The ExoMars Rover and its payload have been therefore designed to investigate the subsurface and drill to collect samples at depths where potential biosignatures could have been preserved.

Among the Rover's payload instruments, the Water Ice Subsurface Deposit Observation on Mars (WISDOM) ground penetrating radar has been optimized to characterize the shallow subsurface over a depth commensurate with the drill capacity (i.e., 2 m) (Ciarletti et al., 2011, 2017). In combination with other instruments onboard the Rover, WISDOM will provide information essential to understand the three-dimensional geological context of the landing site and to choose the best area and depth to collect samples. Furthermore, WISDOM measurements will also play a major role to detect potential buried hazards that might jeopardize drilling activities.

* Corresponding author. LATMOS/OVSQ, 11 bd d'Alembert, 78280, Guyancourt, France.
E-mail address: yann.herve@latmos.ipsl.fr (Y. Hervé).

https://doi.org/10.1016/j.pss.2020.104939
Received 22 November 2019; Received in revised form 5 March 2020; Accepted 12 April 2020
Available online 14 May 2020

The WISDOM instrument has now been manufactured, fully qualified and characterized. In January 2019, it has been delivered to industry for integration on the Rosalind Franklin mission's Rover. Since no calibration of WISDOM will be possible once on Mars, great attention was paid to the datasets acquired during the qualification and characterization tests on Earth. These measurements are crucial for the data processing pipeline that will be used for the data acquired at the surface of Mars.

In this paper, we first describe the scientific and technical objectives, the operating principle and the main components of WISDOM. We then present the qualification and performance tests that have been performed on the instrument flight model and illustrate the obtained results (i.e. end-to-end characterization of the instrument and the required corrections to provide calibrated data). Lastly, we present the anticipated performance of WISDOM once on Mars, the data processing pipeline we have developed including our approach to estimate the ground dielectric constant, and our investigation of the impact of the Rover's structure on WISDOM measurements.

2. Description of the instrument

WISDOM is a dual-polarimetric ground penetrating radar designed to characterize the shallow subsurface of Mars along the ExoMars' rover path.

2.1. Scientific and technical objectives

In order to contribute to the mission's science objectives, the WISDOM radar will be operated before any drilling activity and provide high-resolution images of the shallow subsurface. These radar images, also called radargrams, will extend over a depth ranging from 2 m to 5 m with a vertical resolution of a few centimeters, depending of the subsurface characteristics. They are meant to address the following science objectives:

- Understand the 3D geology and geologic evolution of the site in synergy with surface images acquired by other instruments, such as PanCam (Coates et al., 2017), CLUPI (Josset et al., 2017) and the infrared spectrometer ISEM (Korablev et al.,2017).

This analysis will be based on the buried structures revealed by WISDOM (stratigraphy, spatial heterogeneity…), and on the electrical properties of the detected units (interpreted in terms of physical and compositional properties).

- Investigate the local distribution and state of subsurface water in synergy with the neutron detector ADRON (Mitrofanov et al., 2017) which will provide the bulk hydrogen content of the first meter below the surface.

This includes the search for potential segregated bodies of ground ice and transient occurrence of liquid water/brine at the surface.

- Identify the safest and most promising scientific targets for subsurface sampling and provide an accurate estimate of the depth for the sample acquisition.
- After a drilling, WISDOM will be able to extrapolate in a 2D (or 3D depending on the Rover's path) map the compositional information provided along the vertical direction by the Ma_MISS infrared spectrometer (De Sanctis et al., 2017) located inside the drill.

Given the constraints imposed by the ExoMars mission (in terms of mass, volume, power and antennas accommodation), the design of the WISDOM radar has been optimized to fulfill these scientific objectives: its penetration depth is commensurate with the drill capacity (i.e., 2 m) and its vertical resolution is in line with the accuracy required to collect 3 cm long samples from below the surface.

2.2. Principle of the instrument and first steps of the data processing pipeline

WISDOM is a step frequency radar operating on a broad frequency bandwidth $B = 2.5$ GHz, from 0.5 GHz to 3 GHz (UHF domain). For each sounding, typically a series of $N = 1001$ harmonic pulses of duration$\tau = 1$ ms and central frequency varying from 0.5 GHz to 3 GHz with a step of $\Delta f = B/N = 2.5$ MHz is generated and transmitted by the transmitting antenna. The N resulting electromagnetic waves propagate toward the surface and into the subsurface and are reflected/scattered by permittivity contrasts in the sounded volume. The portion of the waves that returns to the radar is eventually converted into a signal by the receiving antenna. Inside the receiver, for each frequency, the received signal is multiplied by the transmitted signal, low-pass filtered and sampled. The resulting voltage value U is recorded. Therefore, WISDOM raw data for one sounding consists of a series of N values corresponding to the sounded environment's transfer function (TF) for each frequency. Fig. 1 illustrates the principle of the WISDOM data acquisition in the frequency domain.

Note that only the real part of the TF (i.e., the In-phase component) is measured by WISDOM. The choice has been made to measure only the real part because this simplified design reduces the volume and mass of the electronic unit. In the case of WISDOM operating over a large frequency bandwidth, we know that we can retrieve the imaginary part of the Fourier transform computing the Hilbert transform of the real part. The Hilbert transform theoretically requires the knowledge of the real part over an infinite bandwidth. In practical, the 2.5 GHz provides enough information to compute the imaginary part without noticeable errors. Indeed, this has been confirmed by simulations and comparisons with measurements performed with a network analyzer giving access to both In-phase and Quadrature components.

An Inverse Fast Fourier transform (IFFT) is then performed on the frequency domain complex data in order to obtain the response of the sounded volume in the time domain expressed in V. Hz. Before computing the IFFT, classical technics (Hervé, 2019) are used to improve the waveform (see Section 4.4). Namely, zero-padding is used to obtain interpolated data in time domain (we usually use an interpolation factor of 10) and windowing by a Hann window is applied for an easier data interpretation, since it represents a good trade-off between amplitude of the side lobes and resolution. The consequent reduction of the effective bandwidth results in an experimentally observed increase of the pulse width at half maximum to about 0.8 ns, compared to the 0.5 ns value obtained without windowing.

In order to obtain a magnitude in time domain independent of the actual number of samples used in frequency domain, the result of the IFFT must be multiplied by the interpolation factor introduced above. Once combined, successive soundings acquired along a horizontal profile form an image (a radargram) that displays the horizontal and vertical variations in permittivity within the subsurface. By-products, such as an estimate of the surface topography and of the subsurface dielectric constant (real part of the complex permittivity ε_r) can also be obtained. Fig. 2 shows an example of WISDOM data both in the frequency and time domains and illustrates the generation of a radargram.

The theoretical resolution in range $R_V$of WISDOM soundings is driven by the instrument frequency bandwidth (it is equal to $c/(2B)$ in the air) while the unambiguous range (i.e., the maximum range at which the range to a target can be measured unambiguously by the radar) is limited by its frequency step (it is equal to $c/(4\Delta f)$ in the air). For the WISDOM nominal parameter's values ($B = 2.5$ GHz and $N = 1001$) and assuming that the radar is operating over a homogeneous low-loss subsurface with a typical dielectric constant of 4, the resolution in distance is about 3 cm and the non-ambiguous range is about 15 m. In addition, thanks to its step frequency design, WISDOM has no blind zone and the surface echo can thus be used to estimate the dielectric constant of the near-surface (see Section 5.2). The expected performance of WISDOM in terms of penetration depth and resolution are discussed in Section 5.1.

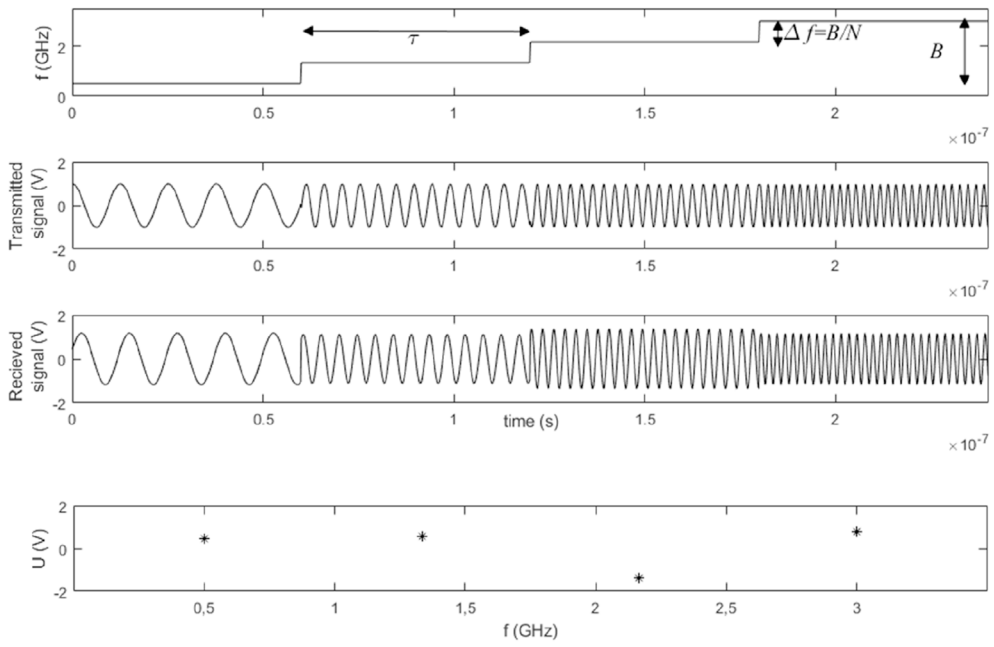

Fig. 1. Principle of WISDOM step-frequency measurements for $N = 4$ frequencies instead of $N = 1001$.

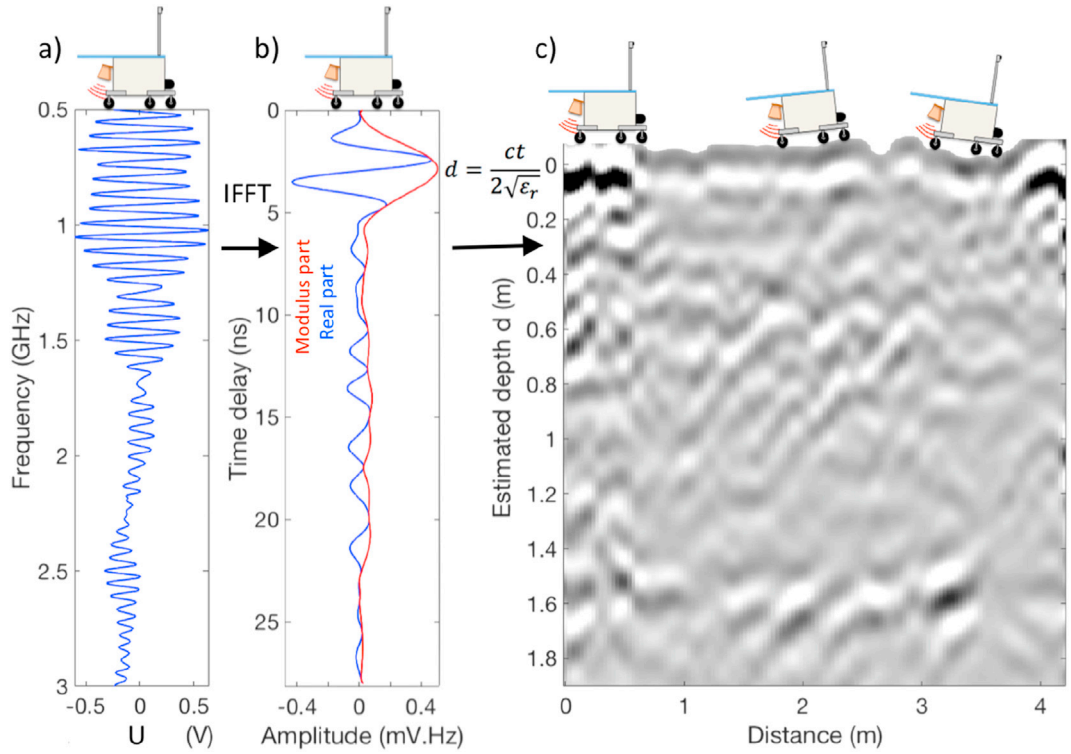

Fig. 2. Generation of a WISDOM radargram. a) Typical signal received by WISDOM in the frequency domain. b) Same signal in the time domain (interpolated by zero-padding) after applying an IFFT. c) Combination of several time domain signals acquired along a 4-m long horizontal profile to build a radargram. Time has been converted into an estimated depth using the indicated formula where c is the velocity of light in vacuum and ε_r is the dielectric constant of the subsurface.

Inside the receiver, for each frequency, the received signal is multiplied by the transmitted signal, low-pass filtered and the resulting value is digitized over 16 bits and recorded. The instantaneous Dynamic Range (DR), which is the ratio between the highest and weakest signal that can be measured by the Analogic to Digital Converter (ADC), is given by the following equation:

$$DR = 20*log10\left(2^{N_{ADC}}\right) \quad (1)$$

where N_{ADC} is the number of bits. The 16 bits WISDOM ADC should provide a theoretical dynamic range of 96 dB. In practice, this maximum value cannot be reached due to imperfections, which introduce noise and distortion. As a consequence, the numbers of bits is reduced and the effective dynamics (as guaranteed by the component manufacturer) is

better than 83 dB with a typical value around 88 dB.

2.3. WISDOM units

The WISDOM radar consists in two main units: WISDOM Electronic Unit (WEU) and WISDOM Antennas Assembly (WAA), connected by coaxial cables (Ciarletti et al., 2011, 2017).

2.3.1. WISDOM electronic unit (WEU)

WEU consists of three stacked modules connected by internal harness. The segmentation in separate modules was conceived in order to minimize electromagnetic interference inside WEU and with other Rover instruments and equipment. Each module is composed of an electronic board integrated in its mechanical frame, and fulfills specific functions:

- the Radio Frequency (RF) module generates the UHF frequencies by steps, transmits and receives the high frequency signals (amplification, polarization selection, mixing, etc.),
- the Digital Processing Unit (DPU) module ensures control of the instrument, generation of a stable clock, data processing, housekeeping monitoring and manages the communication interface with the Rover,
- the DC/DC converter module generates all secondary voltages needed by WISDOM electronics from the primary voltage provided by the Rover.

WEU weights 811 g and its overall size is (L × W × H): 145 mm by 163 mm by 55 mm (Fig. 3).

WISDOM performance numbers (vertical resolution, penetration depth) ultimately depend on the characteristics of the Martian subsurface but the WEU has been designed to allow versatility and to optimize performance thanks to adjustable parameters (number of steps, step duration, number of sweeps, attenuation values in the receiving and transmitting chains, etc.). In particular, the tunable attenuations (31 dB in transmission and 31 dB in reception) are adjusted so that the strongest received echo, coming from the surface under nominal conditions, does not saturate the receiver and exploits the maximum dynamic range of the 16 bits Analog to Digital Converter (a signal of ±32768 Analog to Digital Unit corresponds to ± 3.3 V in physical units and an effective dynamic of 84 dB, see also Ciarletti et al., 2017). In addition, WISDOM signal-to-noise ratio can be improved by performing coherent additions of samples within a frequency step and coherent additions of successive frequency ramps. Therefore, weak signals from deeper structures and interfaces can emerge from the background noise and their signals are more likely to be detected.

2.3.2. WISDOM Antennas Assembly (WAA)

The design of WAA was driven by the requirement of a dual polarimetric two-channel GPR system and the need to cover a wide frequency range from 500 MHz up to 3 GHz (Benedix et al.,2013). It includes two perpendicular linear polarized transmitting antennas and two co- and cross-polar oriented antennas for reception. These and other constraints such as polarization cleanliness, footprint overlap and mechanical requirements led to an antenna design which is based on Vivaldi structures for each single element. More specifically, to achieve dual polarimetry, two perpendicular oriented Vivaldi elements are combined in each of the two dual polarized antenna crosses. The four resulting configurations of measurements are referred to as 00 and 11 for co-polarization and 01 and 10 for cross-polarization (Plettemeier et al., 2017). The transmitting and the receiving antenna are bonded next to each other on a common baseplate as one joint “Antennas Assembly”. The baseplate constitutes the mechanical interface to the Rover. Additional Glass Fiber Reinforced Plastic (GFRP) elements are bonded to enlarge the stiffness of the assembly.

Fig. 3b shows the flight model WAA. The overall size of the assembly is (L × W × H): 410 mm by 200 mm by 180 mm. The RF interface with the coaxial cables is achieved by four SMA connectors (two transmitting, two receiving) mounted on the common baseplate of the assembly.

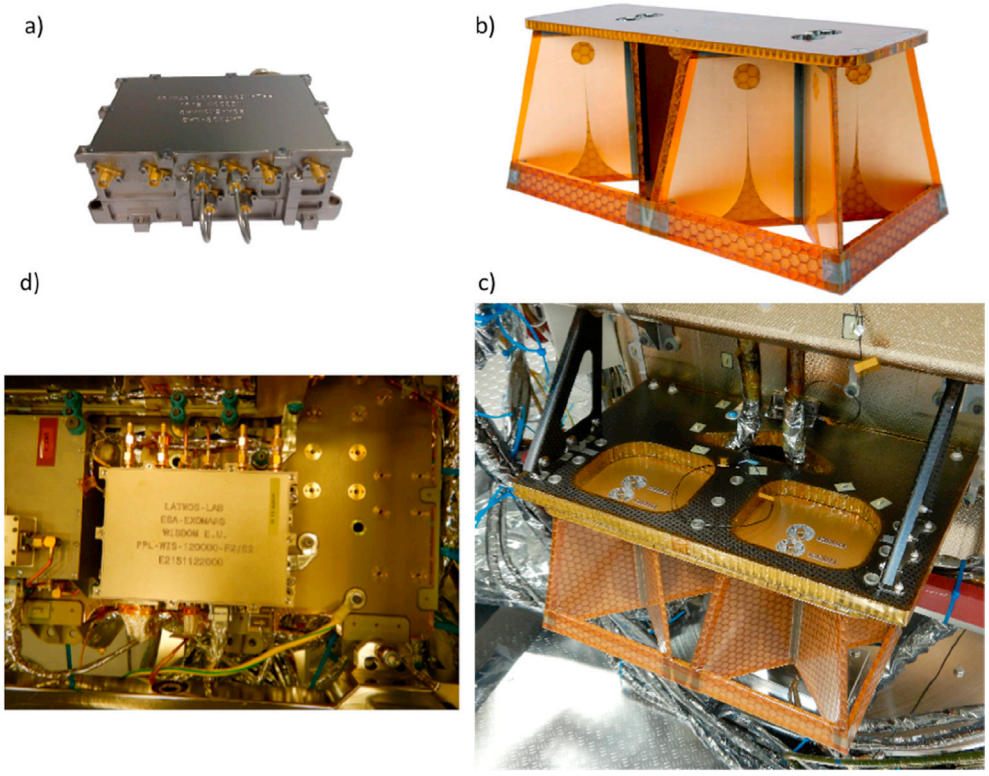

Fig. 3. Left: WISDOM Electronic Unit isolated (a) and accommodated inside the body of the ExoMars 2022 Rover (d). Right: WISDOM Antennas Assembly isolated (b) and accommodated at the rear of the ExoMars 2022 Rover (c). Credits (c & d): Airbus Defense and Space.

3. Qualification of the instrument

3.1. Models of the instrument

The typical implementation cycle of a mission requires building and testing several engineering and qualification models before manufacturing the final Flight Model (FM i.e., the instrument that shall be flown) and its spare (Flight Spare or FS), namely:

- BreadBoards (BB): The BBs are used for design and development of the instrument and are usually not interfaced to any higher level (rover subsystem) for testing purposes.
- Structural/Thermal Qualification Model (STM): the STM shall be representative of the FM design in terms of physical properties: mass (including electrical and optical harness if applicable), mass distribution (center of mass, position), fundamental frequencies and thermo-optical properties, specific heat capacity, thermal conductivity and heat dissipation.
- Electrical Interface Simulator (EIS): the EIS shall be a physical model of the instrument representative of instrument electrical interfaces: interface connectors, electrical and power interfaces, data interfaces, functional interfaces (e.g., operative modes handling in term of interfaces load, traffic and power dissipation).
- Software Interface Simulator (SWIS): the SWIS shall consist of a piece of software having the capability to represent the logical behavior at the communication I/F, exchange TM/TC, provide HK telemetry, provide some predefined science telemetry allowing for data post processing, provide representative failure/anomaly indications
- Engineering Qualification Model (EQM): the EQM shall be able to support a full sequence of qualification testing of the equipment design, inclusive the demonstration that the FM is capable to sustain bioburden control and reduction procedures.

The WAA subsystem followed the sequence described above with the delivery of a full EQM, an FM and an FS. However, for schedule reasons, the WEU subsystem followed a Proto-Flight Model (PFM) philosophy, i.e. no full EQM was developed. The WEU PFM was successfully qualified and delivered, however manufacturing problems led to several reparations, two delta-qualification sessions and potential overstress. It is thus the Proto-Flight Spare (PFS) model of WEU which is integrated on the Rover that will fly to Mars. It was therefore subjected to qualification tests with acceptance durations.

3.2. Overview of the qualification tests

WISDOM instrument underwent a full qualification test campaign to check that it is robust and reliable enough to withstand the stringent mechanical and thermal constraints of a space mission from launch to the end of the nominal operations on Mars. Qualification tests were performed at subsystem level: WAA on the one hand and WEU on the other hand. The WAA being mounted outside the Rover is directly subject to the Martian environment, whereas the WEU is accommodated in the service module inside the Rover body, which is thermally controlled.

The WAA qualification and lifetime tests (>327 cycles for temperatures in the range −130 °C and +80 °C) were performed on the QM of the subsystem. The WAA FM integrated on the Rover that will fly to Mars was subject to acceptance testing (application of lower levels) in the following sequence: performance tests (radiation pattern measurements) in an anechoic chamber, thermal vacuum/Mars environment tests and vibration tests. Cleaning, envelope measurement, mass and inertia center measurements and Dry Heat Microburden Reduction (DHMR) sterilization completed the test sequence before delivery. Functional checks were performed before and after each test.

The WEU PFS full test sequence is depicted on Fig. 4. It includes:

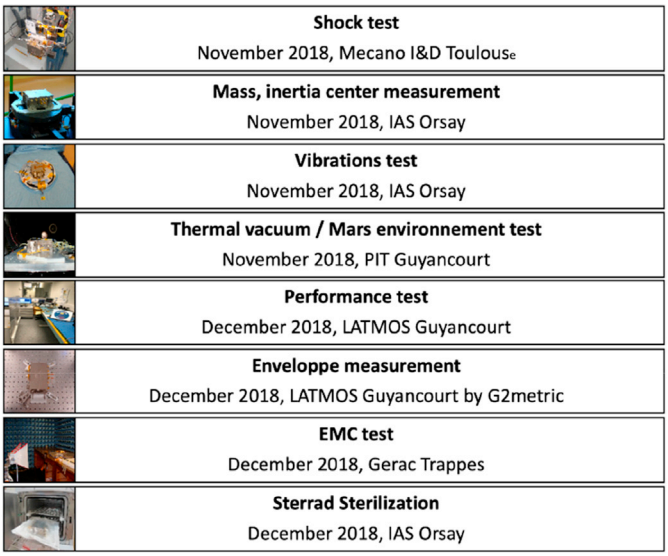

Fig. 4. WEU PFS qualification test sequence.

- Mechanical tests to ensure that the instrument complies with its mechanical design specifications and meets the mission requirements, especially the stringent conditions encountered during launch and landing on Mars:
  - Metrology measurements assess all physical dimensions as well as surface planarity of the instrument.
  - Physical measurements assess the instrument mass, center of gravity and moments of inertia in three axes.
  - Shock tests validate that no degradation occurs after applying shock levels relevant to the mission profile. They are performed on a Shock Response Spectrum Test Bench with dedicated acquisition and analysis system.
  - Vibrations tests assess the instrument resonant frequencies and check that no degradation occurs after applying sine and random vibrations levels in three axes as specified by the mission profile. They are performed on a shaker.
- Thermal vacuum/Mars environment tests (see following section).
- Electromagnetic Compatibility (EMC) tests designed to check that the electrical interfaces (impedance, isolation, bonding) meet the mission requirements, that WISDOM operations will not jeopardize other Rover instrument systems (conducted and radiated emissions) and that WISDOM measurements are not degraded by perturbations coming from other systems (conducted and radiated susceptibility). The EMC tests were performed in an anechoic chamber.
- Sterilization: ExoMars mission has stringent Planetary Protection requirements to prevent particulate, molecular and biological contamination of Mars by components brought from the Earth. Instruments have to be delivered sterile. A hydrogen sterilization based on the Sterrad© process was applied to WEU and DHMR to WAA.

Functional checks of WEU (measurements on 50 Ω RF loads and reference coaxial cables in place of the antennas) were performed before and after each test.

In addition to these qualification tests, calibration of the complete instrument (WEU + WAA) is necessary to assess the instrument performance ("Performance tests" in Fig. 4). It consists of reference measurements on known targets (free space, metallic plate, metallic sphere, etc.). Such measurements were first performed in a cleanroom (see Section 4.4) and a subset of them have been repeated before launch with WISDOM integrated on the mission Rover in order to evaluate the impact of the Rover structure on WISDOM measurements (see Section 5.3).

3.3. Thermal vacuum/Mars environment tests

The data set collected during the thermal vacuum tests in Martian-like environment are essential for a quantitative analysis of WISDOM data. They will be eventually used to correct effects related to temperature variation on the data acquired on Mars and also to ensure that the reference measurements acquired before launch on Earth at room temperature can be used as calibration files for measurements performed during the mission at different temperatures.

The WEU thermal test campaign was conducted in the Mars chamber at the PIT (Plateforme d'Intégration et de Tests) facility in Guyancourt during the two last weeks of November 2018. Its objectives were:

- qualify the subsystem in temperature over the non-operational temperature range by checking its health.
- check that all functionalities are operational during and after the test and that no degradation occurred for operational temperature range.
- characterize the WEU performance behavior, such as the transmitted power as a function of temperature.
- update the WEU thermal model which is integrated in the global Rover's thermal model.

In nominal operations, the temperature on one foot of WEU - which is from the Rover's point of view the Temperature Reference Point (TRP) for WISDOM - is regulated at Rover's level. The temperatures are also monitored on four points inside the WEU (two on the RF board, one on the DC/DC board, one on the DPU board) and the corresponding values are available through WISDOM House Keeping data.

For the thermal tests reported here, WEU was connected to the TF (Transfer Function) box, which is an equipment simulating radar echoes (with adjustable attenuations and delay values) used to perform functional and performance tests. WEU was also equipped with ten additional temperature sensors to monitor the temperature and its spatial variations on the unit. The WEU PFS qualification test condition definition was derived from ExoMars mission specifications and profile:

- one non-operational cycle (instrument OFF) between −55 °C and +60 °C at TRP and one operational cycle (instrument ON) between −50 °C and +60 °C at TRP performed in vacuum (10^{-6} mbar),
- three operational cycles (instrument ON) between −50 °C and +60 °C at TRP performed in Mars conditions (7 mbar CO_2). Tests have been performed for three different power supply voltage values to check potential impact. The last cycle also included intermediate temperature steps for instrument behavior characterization: +55 °C, +40 °C, −5 °C, −30 °C, −49 °C.

The WEU PFS successfully passed the thermal qualification tests.

The following sections apply to the model that will fly to Mars, i.e. WAA FM and WEU PFS and that will be simply called WISDOM.

4. Characterization and calibration of the instrument

The technical objective of the WISDOM radar is to provide accurate measurement of delays that will be ultimately converted into distances and depths, and of amplitudes that will be interpreted in terms of permittivity values for the detected units. To reach this objective, a full characterization of the instrument is necessary both in time and amplitude (Hervé et al., 2019a,b). The main results obtained on the WISDOM flight model are reported in this section.

4.1. Transmitted power and transfer function

In order to be able to convert the signals measured in the frequency domain by WISDOM in Volt into power in dBm, the power transmitted by WEU has been measured with a spectrum analyzer and compared with WISDOM measurements. Fig. 5a shows the power P_t transmitted by WEU and measured with the spectrum analyzer over the whole WISDOM frequency bandwidth for three different values of Tx attenuation in the WISDOM transmission channel. The total attenuation's values considered are 82 dB, 68 dB and 60 dB corresponding respectively to 30 dB, 16 dB and 8 dB attenuations, 22 dB losses in the cables and 30 dB attenuation at reception. We note that the transmitted power changes over the WISDOM bandwidth and that its maximum value is 17 dBm. Furthermore, for the same set of attenuators as mentioned above, we have directly connected the transmitting and the receiving WISDOM channels with a cable and have measured the signal U recorded by WISDOM (see section 2.2) (Fig. 5b). Finally, Fig. 5c displays the power P_t measured by the spectrum analyzer in dBm as a function of the amplitude of the received signal U in Volt plotted in logarithmic scale. It shows that, for each frequency f, there is a linear relationship between these two quantities:

$$P_t(f) = 20\log_{10}U(f)\alpha(f) + \beta(f) \quad (2)$$

where $\alpha(f)$ and $\beta(f)$ are the slope and the origin intercept of the linear relationship at a given frequency f, respectively.

Fig. 6 displays the parameters of WISDOM transfer function,α and β,

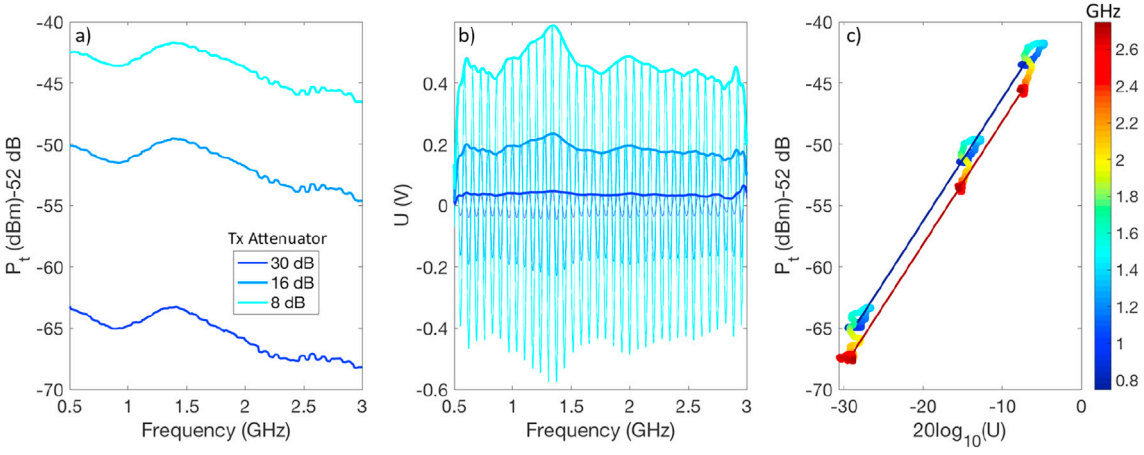

Fig. 5. a) Power transmitted by WISDOM measured by a spectrum analyzer as a function of frequency for different values of the transmission attenuator (30 dB, 16 dB and 8 dB). b) Amplitude (in Volt) of the signal measured by WISDOM for the same values of attenuator as for a). c) Amplitude of the transmitted signal as a function of the power measured by the spectrum analyzer and of frequency (color code) in logarithmic scales. The blue and red lines indicate the best-fit transfer function for 0.8 GHz and 2.7 GHz, respectively. (For interpretation of the references to color in this figure legend, the reader is referred to the Web version of this article.)

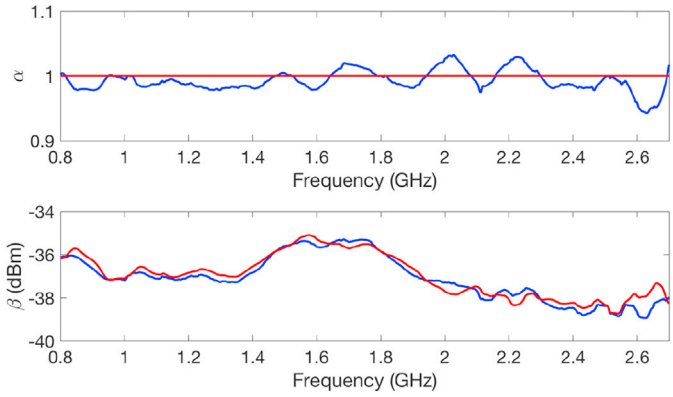

Fig. 6. Parameters α and β of the WISDOM transfer function (see equation (1)) as a function of frequency before (in blue) and after (in red) setting α to 1. The blue curves are used in the following to convert WISDOM data into power. (For interpretation of the references to color in this figure legend, the reader is referred to the Web version of this article.)

as a function of frequency. They were obtained by fitting the three experimental measurement points available (corresponding to three different attenuations) for each frequency with the least-square method as shown on Fig. 5c for 0.8 GHz and 2.7 GHz. We discarded the boundaries of the bandwidth due to the unsatisfying reconstruction of the envelope of the signal at these frequencies. Because the power is proportional to the square of the amplitude, α is expected to be close to 1 as indeed observed (Fig. 6). In the remaining of the paper, we set α to 1 and use the resulting β to get the transfer function that converts WISDOM measurements into dBm.

4.2. Temperature correction

Fig. 7a displays the WISDOM raw data acquired in the frequency domain under low-pressure Martian condition during the qualification tests (see Section 3.3). It shows that the temperature has a significant effect on the amplitude of the signal received by WEU. More specifically, the amplitude decreases with temperature. This decrease corresponds to a power loss about 0.05 dB/K over the WISDOM bandwidth as shown in Fig. 7b, where the temperature is measured on the WEU RF board. This curve will be used to correct variations due to temperature on both the calibration data (i.e., free space and metallic plate measurements) and the data acquired on Mars as follows:

$$U^{\mathrm{corr}}(T_{\mathrm{REF}}) = U(T_{\mathrm{RF}}) \times 10^{\frac{0.0535\ (T_{\mathrm{RF}} - T_{\mathrm{REF}})}{20}} \quad (3)$$

where U expressed in Volts is the amplitude of the raw data, T_{RF} the temperature of the RF board and U^{corr} the temperature-corrected amplitude for a reference temperature T_{REF} arbitrarily chosen which will be typically +33 °C.

For the sake of validation, equation (2) was tested on data acquired during the performance tests in a cleanroom as the RF board temperature was drifting from +25 °C to +45 °C. Fig. 7c shows the amplitude of the direct wave (i.e., the wave propagating in the air) between the transmitting and receiving antennas (also called the antenna crosstalk, see Section 4.3), which is supposed to be constant if the temperature remains constant. As expected, once the temperature effect is corrected, we retrieve a nearly constant signal. Furthermore, an analysis of the data shows that the measured delays are not impacted by temperature variations.

4.3. Antenna main characteristics

After the environmental tests, WAA main parameters such as matching, antenna crosstalk, gains and radiation patterns, were measured in anechoic chamber. In particular, the knowledge about the radiation characteristics of the WISDOM antennas is important for signal processing and data interpretation. Fig. 8a shows the gain in the main beam direction of one WAA radiating element. It was measured in an anechoic chamber and compares very well with numerical simulations. Differences between the four radiating elements were found to be negligible. The gain of the used Vivaldi design increases with frequency until up to 2.6 GHz. This partly compensates the wave divergence and the losses expected in the sounded materials, which both increase with frequency. Above that frequency, side lobes increase through which more energy is radiated in directions other than main beam direction. This is illustrated for two frequencies in Fig. 8c.

For the usable dynamic range of the radar the crosstalk between the transmitting and receiving antennas is also of great interest. This effect (also referred to as antenna coupling) has been measured in an anechoic chamber and proved to be present especially in the lower part of the WISDOM spectrum; it is nevertheless less than −15 dB for frequencies lower than 1.5 GHz and less than −35 dB for frequencies higher than 1.7 GHz (Fig. 8b).

4.4. Waveform and freespace measurement removal

As explained previously, the WISDOM data are acquired in the frequency domain; they are converted into time domain for physical interpretation. Given the WISDOM bandwidth of 2.5 GHz, a Fourier transform leads to a temporal sampling period of 0.4 ns. In order to find a suitable interpolation method, we first needed to better characterize the end-to-end waveform of the whole instrument (transmitting and receiving chains with antennas included). For this goal, we used the signal reflected by a smooth metallic plate (1.5 m × 1 m) and gradually increased the distance D between WAA and the reflecting plate thus the time of arrival of the received signal in order to fill the gap between the 0.4 ns with additional samples. Indeed, applying this stroboscopic method, we performed measurements for a number of distances D ranging from 30 cm to 90 cm with a 1-cm step, corresponding to a temporal step of 0.067 ns (much smaller than the initial 0.4 ns)

The necessary corrections on the amplitude and on the additional delay are applied so that all measured signals can be superposed. The experimental set-up in a cleanroom and the resulting interpolation are presented in Fig. 9. The experimental waveform (Fig. 9b) remains the same within the range of distances considered and it demonstrates that the interpolation of the WISDOM received signals is mandatory to obtain accurate amplitude and delay estimates for the received signals.

Comparison with a waveform interpolated by zero padding (blue curve in Fig. 9b) shows that both methods give very similar results in terms of shape, amplitude and delay. Henceforth, we systematically use zero-padding to perform the needed time interpolation in the data processing chain. The width of the interpolated waveform at half maximum is 0.8 ns when using a Hann window; it corresponds to a propagation distance 10.5 cm in free space. Without any window function, we obtain as expected a narrower pulse with a width of 0.5 ns (7.65 cm in free space), very close to the theoretical vertical resolution (6 cm in free space).

The time domain representation of the data allows us to identify the different echoes and analyze the amplitude and the time of arrival of some particular echoes. When the antennas are 38 cm above the surface (as imposed by the accommodation on the ExoMars 2022 Rover, see Section 5.3), the antenna coupling is the second signal to be received by the instrument, after the internal coupling due to the electronic of the RF board and before the echoes coming from the Rover, the surface and subsurface (Fig. 10). This coupling, as well as the internal coupling and its multiple reflections, will be removed in frequency domain subtracting to the WISDOM raw data a reference measurement corresponding to free space (red curve in Fig. 10). For a better understanding of the effect of this removal the result is displayed in Fig. 10 in time domain.

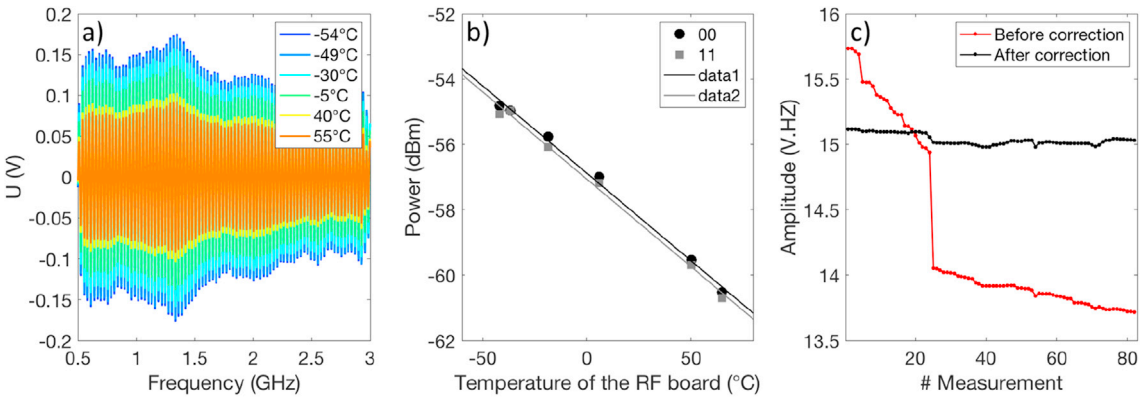

Fig. 7. a) WISDOM measurements acquired during the thermal vacuum tests in Martian-like environment at temperatures ranging from −54 °C to +55 °C (see Section 3.3). b) Power of WISDOM spectra acquired during the thermal vacuum tests in the two co-polarization modes of the instrument (00 and 11) as a function of the temperature of the RF board. c) Amplitude of the direct coupling before and after temperature correction (to a reference temperature of 33 °C).

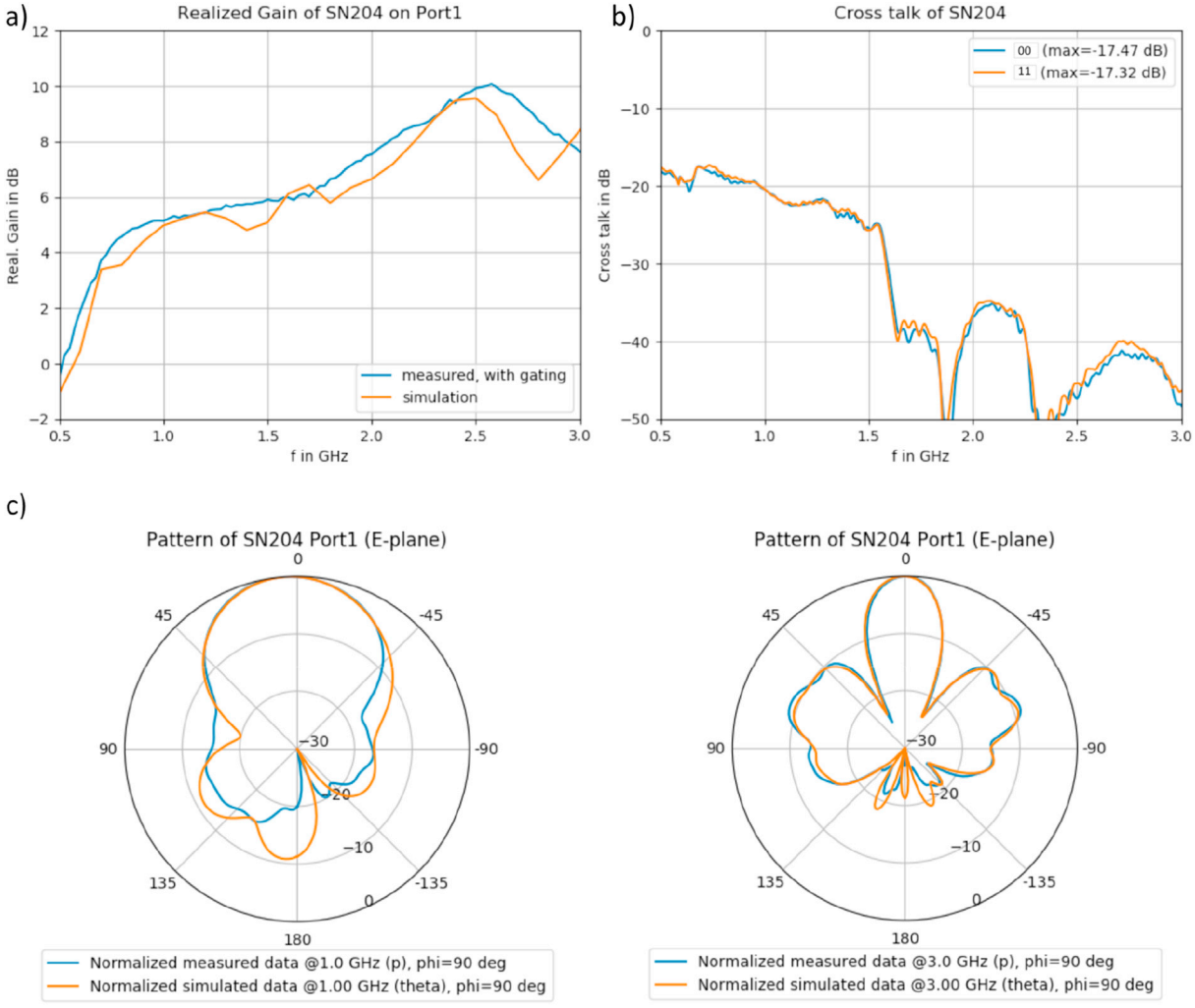

Fig. 8. a) Antenna gain in the main beam direction as a function of frequency. b) Antenna crosstalk (or coupling) as a function of frequency. c) Normalized radiation patterns of one radiating element in E-plane at 1 GHz (left) and 3 GHz (right).

4.5. Experimental determination of the vertical resolution

WISDOM is also expected to provide essential information to guide the sample acquisition operations by the drill. For this technical objective, because the length of the core sample is 3 cm, the vertical resolution achieved by WISDOM should be no more than a few centimeters inside the ground. In order to experimentally measure the vertical resolution actually achieved by the instrument, we performed measurements on two metallic plates separated by a vertical elevation dz. The experimental set-up is depicted in Fig. 11a and produces two echoes separated by a time delay equal to $2dz/c$. Fig. 11b illustrates the results in time domain for a dz value of 7 cm.

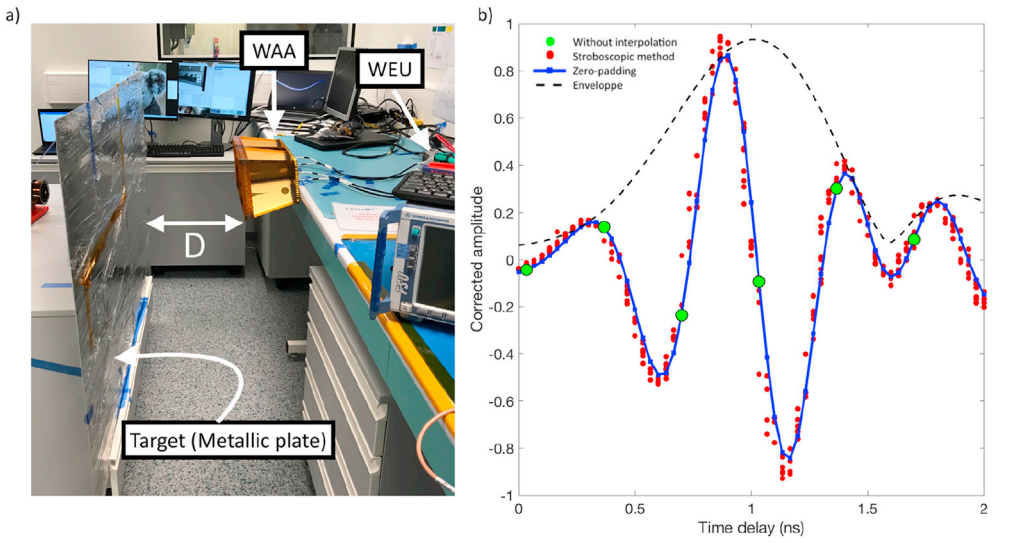

Fig. 9. a) Experimental set-up inside the clean room of the PIT facility in Guyancourt, France. b) Reconstitution of the waveform by the experimental stroboscopic method (red) and zero-padding numerical method (blue) from the values measured by WISDOM (green). The data presented here have been filtered before inverse Fourier transform with a Hann window function. (For interpretation of the references to color in this figure legend, the reader is referred to the Web version of this article.)

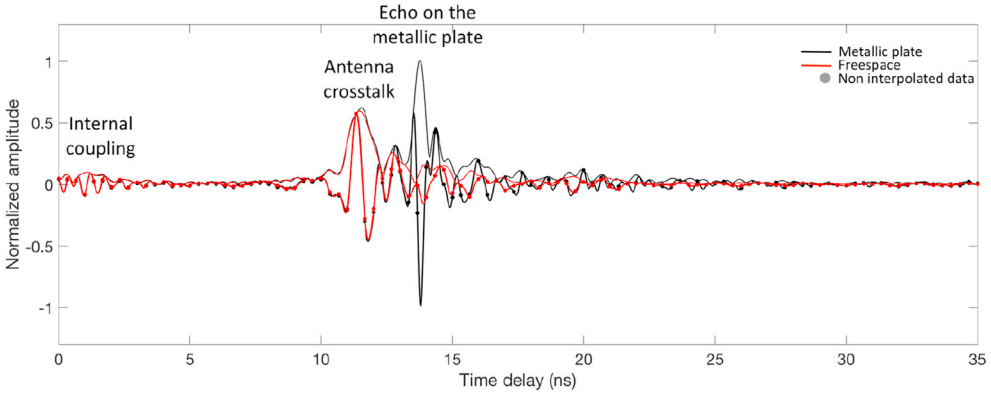

Fig. 10. Illustration of WISDOM measurements in free space and above a metallic plate in the time domain (located at 42 cm from WAA), acquired in the Airbus sterile room with the instrument fully integrated in the Rosalind Franklin Rover. Both measurements show the signature of the internal and antenna couplings, which can be removed by subtracting the free space measurement. No window function was applied before the inverse Fourier transform.

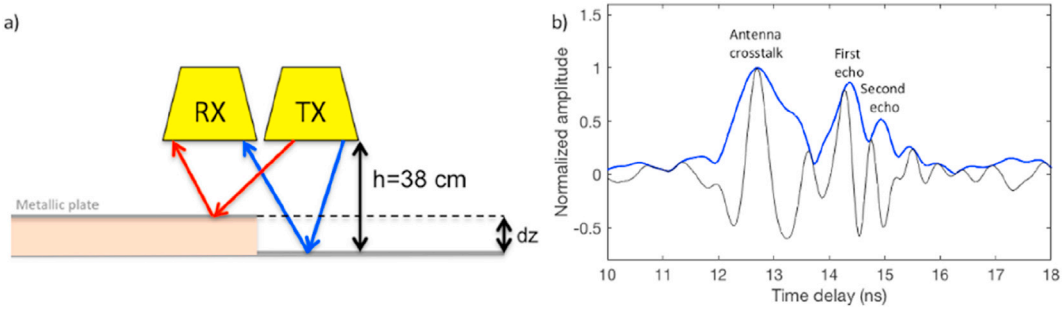

Fig. 11. a) Overview of the experimental set-up. b) WISDOM measurement corresponding to $dz = 7$ cm.

The data collected show that we are experimentally able to distinguish two echoes of a same order of magnitude with good accuracy (<20% relative error on the retrieved delay) until $dz = 6$ cm, which corresponds to a delay of 0.4 ns. This result is expected to be reached when the width pulse at half maximum is not larger than 0.4 ns corresponding to an effective bandwidth of 2.5 GHz which is the instrument total bandwidth.

In the frame of the ExoMars mission, for a Martian subsurface with a typical permittivity value of 4, the achieved vertical resolution in the subsurface is thus expected to be around 3 cm. This result is in line with the ExoMars requirements linked to the sample acquisition.

4.6. Link budget analysis

As already described in Section 4.4, measurements performed at different distances from a metallic plate are available. In this section, we focus on the amplitude A of the signal reflected by the plate. Fig. 12a presents a schematic view of the experimental set-up including information on the range of gain/loss in each component of the radar.

Fig. 12b displays the amplitude A of the reflected signal in the time

domain as a function of the distance D between the metallic plate and the antennas. Despite the fact that the distances considered do not correspond to far-field region configurations for the whole frequency bandwidth, the amplitude A decreases with the distance following a model of equation (4) in which it is inversely proportional to the distance with an additional off-set distance d_0 to be determined.

$$A(D) = \frac{A_0}{D + d_0} \tag{4}$$

Two regions are indentified. For $D > 40$ cm, d_0 is equal to 21 cm and $A_0 = 14.15$ V.Hz.m (red curve on Fig. 12b). When $D < 40$ cm, the same law still gives a good fit with $d_0 = 67$ cm and $A_0 = 24.41$ V.Hz.m (blue curve on Fig. 12b).

These measurements are also useful to validate our knowledge of the WISDOM end-to-end behavior. We have used them to perform a link budget analysis aiming at retrieving the reflection coefficient on a metallic plate (known to be equal to one in absolute value). Performed in the frequency domain, this analysis is crucial since it demonstrates our ability to measure the reflectivity of the surface over the whole frequency range, to deduce the permittivity value of the reflecting bodies and therefore to characterize the detected units in terms of structure (i.e., roughness) and composition (see Section 5.2).

In the case of a smooth and theoretically infinite target interface between two semi-infinite homogeneous media, the received power P_r in far field can be obtained combining the Friis formula and the image theory (Friis et al., 1957; Ulaby et al., 2014) as follows:

$$P_r = P_t G_t G_r |\Gamma|^2 \left(\frac{\lambda}{4\pi\,(D_t + D_r)}\right)^2 \tag{5}$$

Where P_t the transmitted power G_t and G_r are the gains of the emission and reception channels, respectively; they include the antenna gain in the direction of observation (see Section 4.3). D_t and D_r are the distances from the transmitting and receiving antennas to the target, respectively, λ is the transmitted wavelength, and Γ is the target's reflection coefficient. We expect $|\Gamma|$ to be equal to 1 for a large-enough perfectly reflecting plane surface.

The far field limit is frequency dependent. For WISDOM, the antenna design is a complex one but we can estimate that the far field for the whole frequency bandwidth is around 1.6 m. As a consequence, the surface which is 38 cm away from the antennas is not in the WAA's far field.

Nevertheless, we have shown that the amplitude received by WISDOM inversely proportional to a distance which is not the distance D but $D + d_0$ (see equation (4)).

We thus decided to apply the Friis equation with distances $D_t = D_r = D + d_0$ to account for the additional distance d_0 previously determined. For the antenna gains, we consider that $G = G_t = G_r$.

The reflection coefficient of the target is thus given by:

$$|\Gamma| = \sqrt{\frac{P_r}{P_t}}\left(\frac{8\pi(D + d_0)}{G\lambda}\right) \tag{6}$$

Fig. 13 shows the results of equation (6) applied to the whole set of measurements performed on the metallic plate. While we can observe some discrepancy at the edges of the WISDOM bandwidth, the average of the retrieved reflection coefficient $|\Gamma|$ is 0.97 ± 0.09 over the central 0.9–2.3 GHz frequency range. This result is very close to 1 and therefore validates our good knowledge of the characteristics of the different components of the instrument over most of the frequency bandwidth and the fact that we can use the amplitude of the signal reflected by the surface, when roughness can be neglected, to estimate the permittivity of the top layer.

4.7. Noise and signal to noise ratio (SNR)

During the environmental tests, the noise level of the WEU was measured at different temperatures. The observed SNR values are between 82 and 87 dB for a temperature ranging from −54 and + 55 °C in agreement with the expected ADC performance about 84 dB (see section 2.2).

The noise power (P_N) of the whole instrument (antennas included) has been experimentally estimated in the frequency domain. For that purpose, we used measurements performed in the clean room (see Section 4.4) on a metallic plate. The constant signal corresponding to direct coupling, reflections on the plate and on the numerous surrounding reflecting structures can be easily removed by subtracting the mean value computed on the set of measurements. The transfer function determined above (see Section 4.1) is then used to estimate the power of the remaining noise (in dBm).

Fig. 14 shows the observed noise power is relatively flat over the full frequency bandwidth and ranges between −80 and −85 dBm. Coherent additions performed on the data do improve the SNR. However, experimentally, we observe that the additions are less efficient than expected in the presence of an additive white noise. More specifically, 10 additions lead to a gain of 9 dB on the SNR instead of the 10 dB expected. This is due to the fact that unwanted coherent signals are present (likely due to internal reflections).

5. Once on Mars

The instrument has been designed to probe the Martian subsurface. In order to guide the drilling operations, WISDOM is expected to

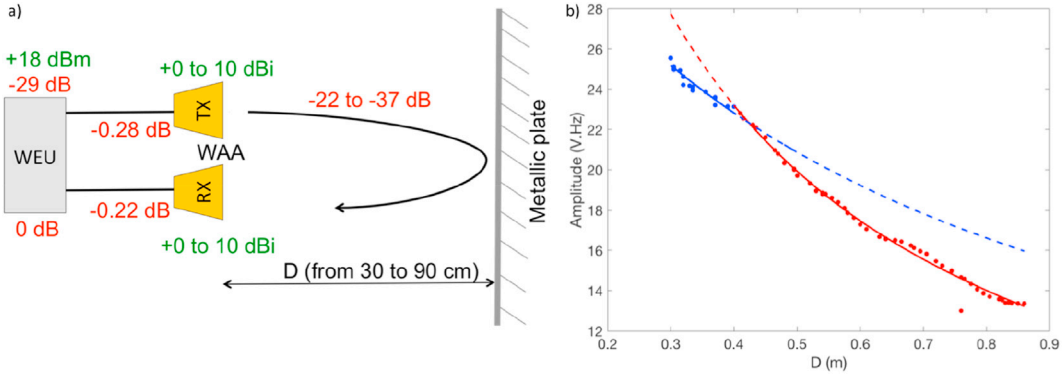

Fig. 12. a) Schematic view of the experimental set-up including information about the losses (in red) and power/gains (in green) in WEU, cables, WAA and air. Ranges are given where losses and gains vary with frequency. b) Amplitude in time domain of the echo from the metallic plate as a function of the distance between WAA and the target. The least mean square-fit models (equation (3)) for $D > 40$ cm and $D < 40$ cm are indicated by red and blue solid lines, respectively. (For interpretation of the references to color in this figure legend, the reader is referred to the Web version of this article.)

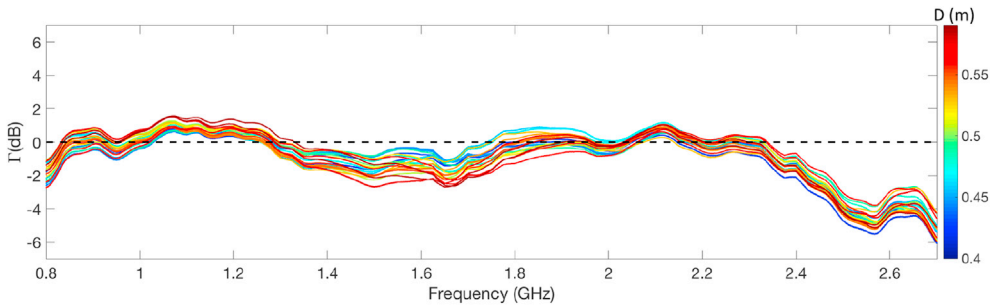

Fig. 13. Retrieved reflection coefficient of a metallic plate as a function of frequency for a series of distance D values between the plate and the antennas.

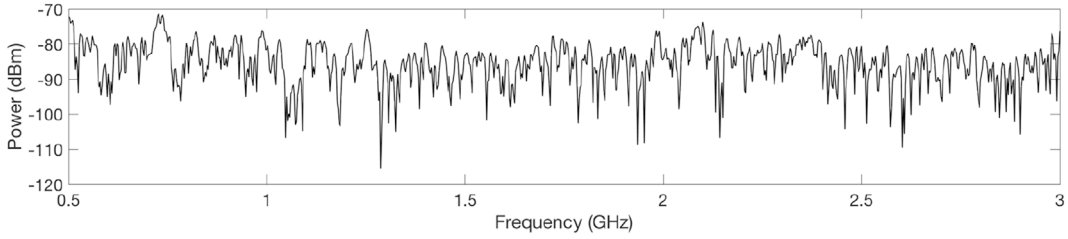

Fig. 14. Noise power determined from measurements on a metallic plate.

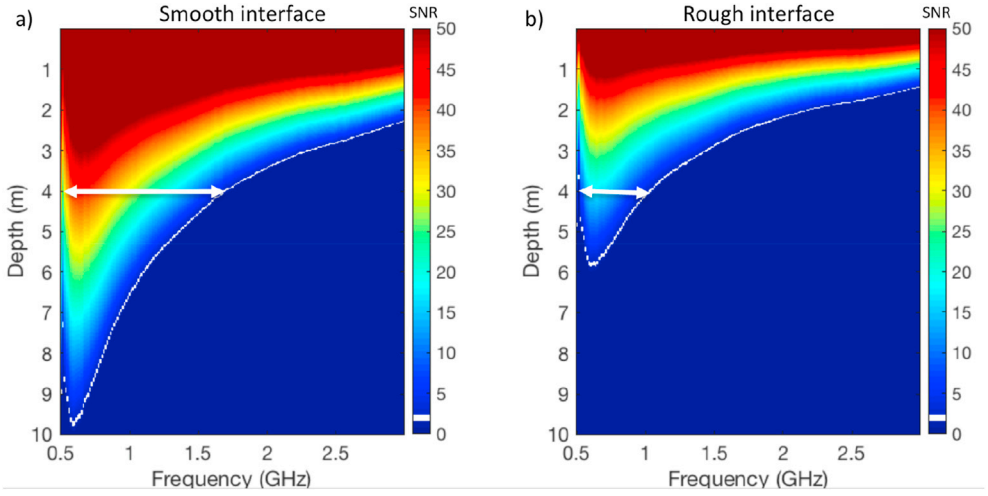

Fig. 15. Map of SNR values as a function of the frequency and depth for a smooth (a) and for a rough (b) buried interface. The curves corresponding to SNR = 3 dB are highlighted in white. The top layer of the subsurface has a real part of the permittivity of 4 and an imaginary part of 0.1 (see Table 1).

characterize the subsurface down to a depth of 2 m with a resolution of few centimeters. Realistic estimates of the instrument behavior and performances in a given environment can be obtained by analytical or numerical models.

5.1. Anticipated performances

Assuming a simple model of subsurface composed of two homogeneous layers separated by an interface, the depth at which the buried interface can be detected by WISDOM and the corresponding vertical resolution can be analytically estimated for different physical states of the interface (smooth or rough). Such an analysis was already conducted based on assumptions made before the final model of WISDOM was actually built and characterized (see Ciarletti et al., 2017 for a detailed description of the method). The recent performance tests conducted on the flight model provided the experimental parameter values required to update this analysis.

For a smooth interface buried at a depth d, the reflection is specular. The received power is given by:

$$P_{r(smooth)} = T_{1/2}T_{2/1}R_{2/3}P_tG^2\left(\frac{\lambda}{8\pi d}\right)^2 e^{-2\frac{\pi\varepsilon''_r}{\lambda\sqrt{\varepsilon_r}}2d} \quad (7)$$

where $T_{1/2}$ is the transmission coefficient air/ground, $T_{2/1}$ the transmission coefficient ground/air and $R_{2/3}$ the reflection coefficient at the buried interface. All three coefficients can be estimated using Fresnel coefficients at nadir. The term $e^{-2\frac{\pi\varepsilon''_r}{\lambda\sqrt{\varepsilon_r}}2d}$ is the attenuation in the layer due to electrical losses.

For a rough interface, we use the radar equation and consider that the contribution of the interface is limited to the first Fresnel zone (Grimm et al., 2006; Cook, 1975) which gives

$$P_{r(rough)} = T_{1/2}T_{2/1}R_{2/3}P_tG^2\frac{\lambda^2}{(4\pi)^3}\frac{1}{2d^4}\frac{\pi\lambda d}{2}e^{-2\frac{\pi\varepsilon''_r}{\lambda\sqrt{\varepsilon_r}}2d} \quad (8)$$

Rather than the received power, the SNR characterizes the ability to detect the signal reflected by the buried interface.

Table 1
Range and nominal values used to compute the SNR values presented in Fig. 15.

		Range	Nominal values
Wavelength in vacuum	λ	0.1–0.6 m	
Transmitted power (Fig. 5a)	P_t	−11 dBm to +18 dBm	−11 dBm
Antenna gain in the main direction (Measurement in anechoic chamber, Fig. 8)	G	1–8 dB	
Noise power (Estimated in section 4.7 from measurements)	P_N	−85 dBm	
Real part of the permittivity of the top layer (Ciarletti et al., 2017)	ε_r	2–5	4
Imaginary part of the permittivity of the top layer (Ciarletti et al., 2017)	ε_r''	0.01–0.5	0.05–0.1 – 0.5
Transmission coefficient air/top layer (Computed)	$T_{1/2}$	0.11–0.44	0.36
Transmission coefficient top layer/air (Computed)	$T_{2/1}$	0.11–0.44	0.36
Reflection coefficient on the buried interface (Computed)	$R_{2/3}$	0.18	0.012

$$SNR = \frac{P_r}{P_N} \tag{9}$$

where P_N is the power of the noise. We took $P_N = -85$ dBm for a reference temperature of +33 °C (see Section 4.7). A signal can be unambiguously detected if the SNR is larger than 3 dB.

The parameter values used for the analysis are given in Table 1.

Fig. 15 shows the SNR values computed with equation (7) for a smooth buried interface and with equation (8) for a rough buried interface. In both cases, moderate electrical losses ($\varepsilon_r'' = 0.1$) and a dielectric constant of 4 are considered for the homogeneous top layer.

In the following, we consider that only signals with a SNR above 3 dB contribute to the interface detection. Regardless of the interface roughness, when the interface depth d increases, the received power decreases. The effect is enhanced for the highest frequencies that are more rapidly attenuated than the lowest ones. The effective bandwidth of the received signal is consequently reduced which leads to a deterioration of the vertical resolution (see Section 2.2).

As an illustration, the white arrows on Fig. 15 a and b show that, for an interface located at a depth of 4 m, the effective frequency bandwidth is 1 GHz for the smooth interface and 0.5 GHz for the rough interface. The corresponding vertical resolutions are respectively 7,5 cm and 15 cm.

Fig. 16 presents a revised version of Fig. 3 from Ciarletti et al. (2017) displaying the depth of the detected interface (corresponding to an echo with an SNR>3 dB) and associated vertical resolution for different properties of the subsurface.

The orange curves are obtained using Fig. 15. The black dots correspond to the configuration at 4 m previously analyzed leading to the resolution values of 7.5 cm and 15 cm.

As expected, the instrument performance depends very much on the subsurface characteristics. In the most favorable but still geologically plausible case (smooth interface and low losses), the detection of the buried interface is possible down to 8 m with the best resolution of 3 cm. In the worst case (rough interface and high losses), the buried interface is detected down to 1 m with the best resolution or down to 2 m but with a vertical resolution degraded to 10 cm.

5.2. Estimation of the ground dielectric constant

Regardless of the attenuation in the subsurface, the surface echo will always be detected by WISDOM. One of the main steps of the data analysis will be to characterize the surface roughness and estimate the dielectric constant value of the top layer. This last parameter provides insights into the composition (including the porosity of the materials) of the subsurface and is also required to convert the measured time delays

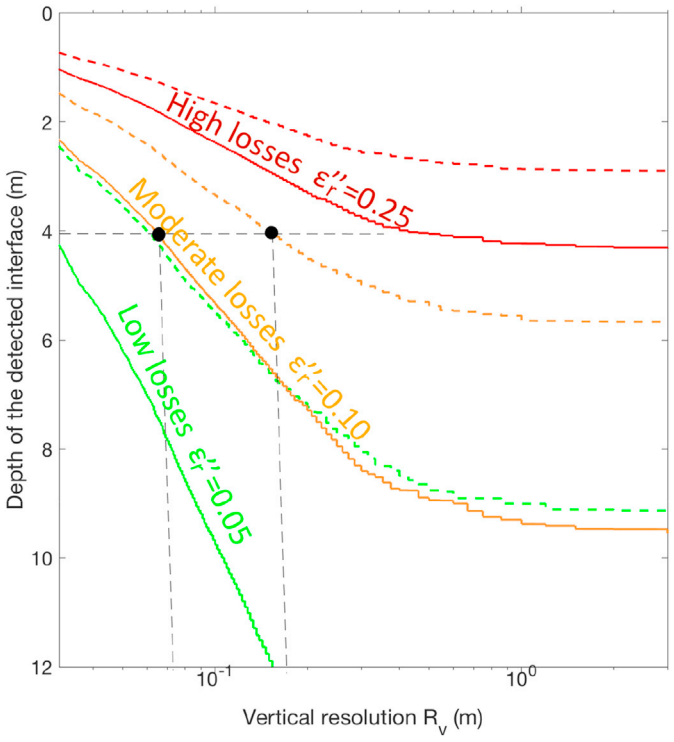

Fig. 16. WISDOM expected performance in terms of depth of a detectable interface and associated vertical resolution for different subsurface properties. The color code indicates the level of electrical losses in the top layer of the subsurface (the real part of the dielectric constant is set to 4, see Table 1). The plain curves are for a smooth buried interface and the dashed ones are for a rough buried interface. (For interpretation of the references to color in this figure legend, the reader is referred to the Web version of this article.)

into distances. A commonly used method to estimate ε_r is based on the analysis of the shape of the hyperbolic signature of buried reflectors (e.g., Overmeeren et al., 1979; Garambois et al., 2002) but the method we propose here relies on the analysis of the amplitude of the surface echo (e.g., Benedetto et al., 2017; Dorizon et al., 2015; Maser and Scullion, 1991; Saarenketo, 2000; Huisman, 2003).

Provided that the surface is smooth, in the far field domain, its reflexion coefficient at nadir is related to the dielectric constant ε_r of the top subsurface layer as follows:

$$\Gamma = \left(\frac{1-\sqrt{\varepsilon_r}}{1+\sqrt{\varepsilon_r}}\right)^2 \tag{10}$$

Equation (5) provides a valid method to estimate Γ and therefore ε_r (if we exclude the fringes of the bandwidth). However, to avoid any remaining uncertainties due to a non-perfect knowledge of the instrument transfer function, ε_r can also be derived using a reference measurement and relying on the fact that the reflected power is proportional to $|\Gamma|^2$:

$$P_r = K|\Gamma|^2 \tag{11}$$

where K is a constant depending on the radar settings and geometrical configuration of operation; it can be experimentally determined from a reference measurement on a metallic plate (for which $|\Gamma|^2 = 1$)

$$K = P_r^{\text{ref}}, \tag{12}$$

it results:

$$|\Gamma|^2 = \frac{P_r}{P_r^{ref}}, \tag{13}$$

and

$$\varepsilon_r = \left(\frac{1 + \left(\frac{P_r}{P_r^{ref}}\right)^{1/2}}{1 - \left(\frac{P_r}{P_r^{ref}}\right)^{1/2}} \right)^2 \tag{14}$$

Just as Γ (see Section 4.6), ε_r can be derived as function of frequency. This would give a unique insight into the level of roughness of the surface at different scales and/or to the electrical properties of the top layer.

Once on Mars, we will thus use a reference measurement performed before launch at the nominal distance of 38 cm on a metallic plate. However, the actual distance between WISDOM antennas and the surface will vary depending on the topography of the landing site and also because the Rosalind Franklin Rover's wheels are flexible and will undergo a squeezing under Martian gravity which is different than the one observed on Earth. The actual elevation of the antennas above the ground will be estimated from the time delay of the surface echo. Prior to the dielectric constant derivation, we will therefore correct the amplitude of the surface echo back to the reference distance of 38 cm using equation (4). This correction is mandatory because the impact of an error of 5 cm–10 cm in the distance would result in a 20% error on the permittivity value and, in turn, in a 10% error on the estimated depths.

Once the amplitude is corrected for the actual distance between WAA and the surface, the accuracy on the permittivity value retrieved is linked to the accuracy on the surface echo's amplitude. Measurements performed with a stationary configuration show that the dispersion of the amplitude value is very low, as low as 0.1% during the thermal vacuum test. Similar measurements on a metallic plate show a dispersion of the amplitude of echo on the metallic plate of about 0.6% (after temperature correction). In conclusion, once the temperature and elevation corrections are performed, the accuracy on the estimated permittivity value is 13%, which results in a 6% accuracy on the estimated depths.

5.3. Impact of the Rover on WISDOM measurements

Finding a suitable location to accommodate WAA on the ExoMars 2022 Rover has been a challenge because, ideally, no Rover part should be in the antenna field of view but, at the same time, the bottom of WAA could not be closer to the surface than the lower part of the Rover body for safety reasons. These constraints were rapidly identified as incompatible due to the wide radiation pattern of the antennas required to correctly map the subsurface. As a compromise, it has been decided that WAA would be accommodated on a bracket at the rear of the Rover and be tilted backwards by 8°. Nevertheless, we anticipated that the Rover structure may have a non-negligible impact on the WISDOM measurements and that is the reason why tests have been performed to accurately characterize the Rover contribution with the intent to remove or reduce its effect by post-processing or, at least, to avoid misinterpretations once on Mars.

5.3.1. Impact of the Rover body

The tests and results reported in this section have been obtained during the preparation for the operation simulation campaign ExoFiT in Chile in February 2019 (Hall et al., 2019). The WISDOM model used for these tests is the FS2, which is a replica of the PFS model that will fly to Mars. The FS2 has been built to perform tests and investigations that could not be conducted with the PFS, which was sterile and, in any case, not available anymore after its integration on the Rosalind Franklin Rover. The Rover model used for the tests is called Charlie; it is similar to the ExoMars 2022 Rover (i.e., it has the exact same wheels) though with a slightly smaller body (by 10%). The tests were run in an area of the Airbus Mars yard in Stevenage (UK) over a ground that displays a simple subsurface structure (namely ~35 cm of reddish sand above a thick layer of concrete).

Fig. 17a shows the experimental set-up used in order to investigate the impact of the Rover body on WISDOM measurements. During this test, the WAA was not accommodated on the Rover but instead held at its nominal elevation from the surface (38 cm) by a cardboard box (transparent for UHF waves). Soundings were performed while the Rover was slowly moving towards the WAA from a distance of 4.5 m (where the influence of the Rover can be regarded as negligible) until it reaches its nominal position (i.e., the closest position as if WAA was actually accommodated on the Rover). This way, reflections due to the Rover could be clearly detected following their decreasing propagation delay and increasing amplitude (see the radargram on Fig. 17b).

On Fig. 17b, the first sounding performed at a distance of 4.5 m has been subtracted from all other soundings in order to better highlight what is only due to the Rover displacement. Two types of signals then remain; they originate from either (i) direct reflections on the Rover structure or (ii) multiple reflections involving both the surface and the Rover structure. In order to discriminate between these two types of signals, the same measurements have been performed over a thin metallic plate (not shown here). The reflection on the metallic plate is about three times stronger than on the sand therefore type (ii) reflections show a much stronger amplitude in presence of the metallic plate than without while type (i) reflections are similar in both cases. This is how we have identified two strong signals (white arrows in Fig. 17b) corresponding to the direct reflection on the Rover structure.

During WISDOM operations on Mars, WAA will be moving along with the Rover and any reflection on static parts of the Rover structure will result in horizontal lines constant in amplitude on the radargrams; these parasitic signals can be easily removed by subtraction. In contrast, weaker signals involving an interaction between the Rover and the surface will vary in amplitude and arrival time as a function of the surface properties. Signal and image processing algorithms based on correlation with the surface echo may help reducing their impact.

5.3.2. Impact of the Rover wheels

Attention was also paid to the possible impact of the Rover rear wheels on WISDOM data. A first dedicated test was run with WAA mechanically mounted on the Charlie Rover (which carries the exact same wheels as the Rosalind Franklin Rover) slightly lifted from the ground. Soundings have been performed while the wheels were slowly rotating in order to capture any changes due to reflections on parts of the wheels. The data indeed show weak but noticeable periodic features related to the wheels' rotation. The effect is also visible in cross-polarization measurements which is consistent with the fact that the structures on the wheels are angular and thus depolarizing.

At the end of August 2019, the calibration and characterization tests performed with WISDOM integrated on the mission Rover provided the unique opportunity to characterize the performance of the instrument in its final operation configuration. Due to stringent restrictions inside the sterile rooms where the ExoMars Rover was being integrated and tested, there were limitations in the tests that could be performed. These tests nevertheless provide mandatory reference measurements. In particular, a series of soundings were performed with the Rover lifted to more than 1 m from ground (see Fig. 18) in order to obtain a "free-space" measurements including the impact of Rover's parts. Soundings on a flat metallic plate were also conducted; they will serve as the reference measurements mentioned in Section 5.2. All these reference data will be integrated in WISDOM automatic data processing pipeline.

Measurements with spinning wheels have also be performed in order to characterize their impact on the WISDOM data. The radargram presented in Fig. 18b has been acquired in the same configuration as that of Fig. 18a, while rotating the wheels. All constant signals have been removed from the radargram; therefore, the periodic features in the image are due to reflections on the wheels. Future work will be dedicated to develop algorithms that will be able to reduce as much as possible this

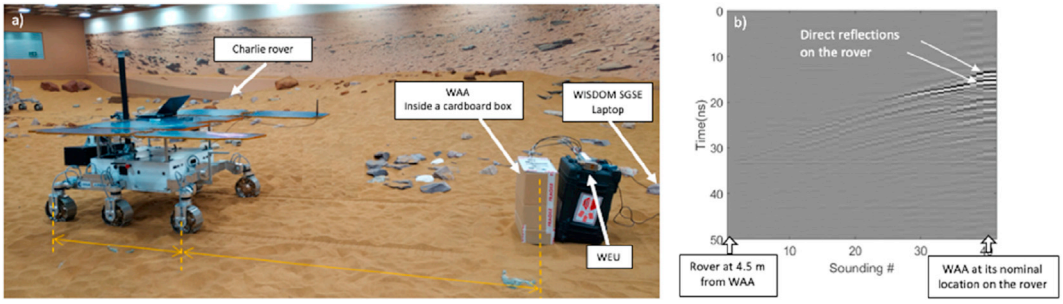

Fig. 17. a) Experimental set-up with the ExoFiT Charlie Rover in the Airbus Mars yard. WAA is held in place inside a cardboard box. The distance between the Rover and WAA is approximately 2 m. b) Radargram showing the reflections due to the Rover structure as the Rover gets closer to WAA.

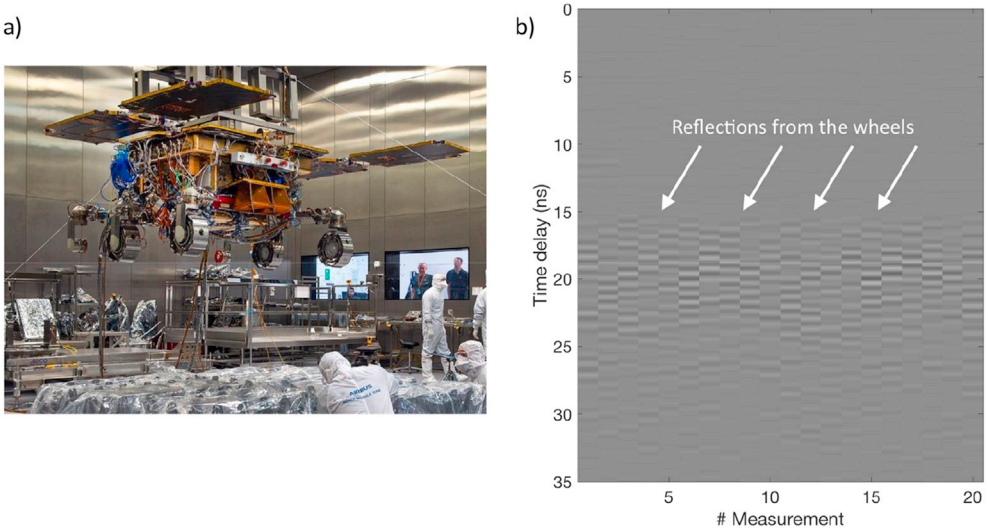

Fig. 18. a) Rosalind Franklin ExoMars Rover at Airbus Defense and Space Bio Clean Room, Stevenage (UK) during the calibration tests for WISDOM. The Rover is lifted and the ground is partially covered by absorbers to reduce parasitic reflections. Copyright: Max Alexander/Airbus. b). Radargram obtained from soundings with a configuration where the rotating wheels are the only moving parts.

effect.

5.4. Data processing pipeline

Taking into account all the information available on the instrument a set of tools have been designed to extract the best from the WISDOM dataset. Fig. 19 summarizes the steps that are integrated in the chain designed to automatically process the WISDOM data and produce calibrated radargrams. During the operations on Mars, this automatic processing will have to be executed in less than 20 min. Another 20 min can be allocated to manually run codes when the automatic processing does not seem to be well adapted to the dataset or when especially interesting features are detected and require a more sophisticated analysis. The processed data will contribute significantly to the decision-making process regarding the next steps of the ExoMars 2022 Rover on Mars. The raw and processed data at different levels will be archived as well as more elaborated products such as permittivity values and distribution of buried boulders size to be in time made available for the scientific community.

6. Conclusion

The WISDOM radar has been designed and built to answer the technical constraints and scientific goals of the ExoMars Rover mission; it will provide a description of the first meters of the Martian subsurface with a vertical resolution of a few centimeters. WISDOM observations will be essential to understand the geological context of Oxia Planum, the ExoMars 2022 landing site, and to select relevant and safe locations for subsurface sample collection.

The WISDOM flight model went through a series of qualification tests on line with the mission's profile before it was delivered and eventually tested in the Airbus sterile room once fully integrated on the Rosalind Franklin Rover. All performed calibration tests will greatly help to interpret future WISDOM data and have been included in the data processing pipeline of the instrument.

WISDOM automatic data processing pipeline has been designed to run in less than 20 min as requested by ESA to rapidly provide the information required to plan drilling operations once on Mars. A more sophisticated pipeline is in development; it includes automatic detection of subsurface structures and a high-resolution algorithm based on the bandwidth extrapolation method (Cuomo et al., 1992; Raguso et al., 2018) which will significantly improve the vertical resolution of WISDOM radargrams (Oudart et al., 2019).

In depth analysis of the WISDOM data will also rely on the synergy with other instruments of the Rover. In particular, WISDOM and PanCam joint observations should provide a 3D representation of the investigated site including both surface and subsurface. Synergy with Ma-MISS (once the drilling operations has been performed) and with ADRON (for the analysis of any potential water content with depth) are also anticipated and should greatly enhance the scientific return of the ExoMars mission.

WISDOM took part in 3 operation simulation campaigns during which several instruments of the ExoMars Rover were operated from a remote control center to test and improve the efficiency of the data processing pipeline, decision-making process and operation planning under conditions similar to those expected during the ExoMars mission (Ciarletti

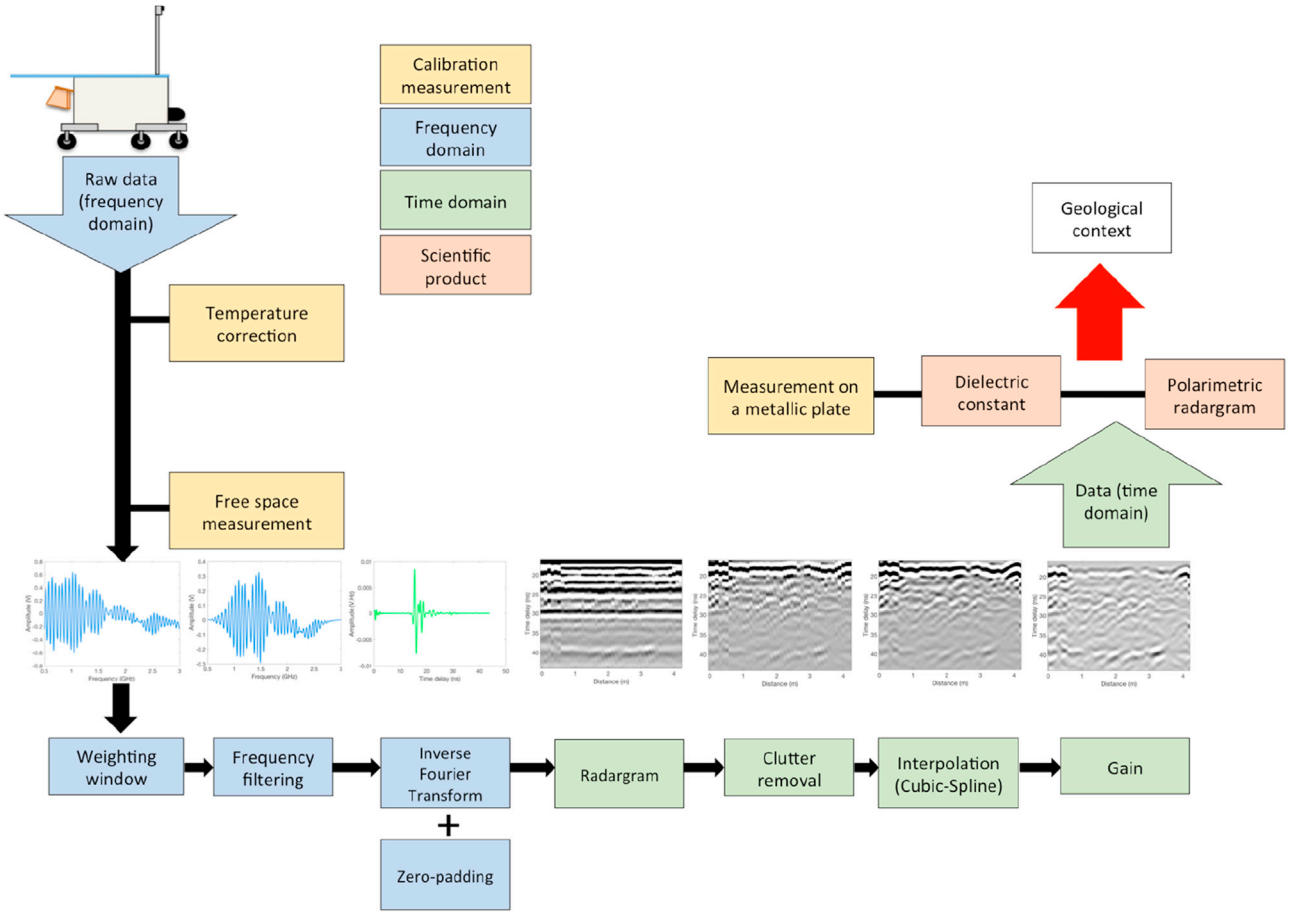

Fig. 19. Schematic of the automatic data processing chain developed for WISDOM data.

et al., 2017; Joudrier et al., 2012; Gunes-Lasnet et al., 2014). During the latest of these simulation operation field trials, ExoFit 2019 (Hall et al., 2019), a flight-like version fully representative of the WISDOM flight model was mounted on a rover in the Atacama Desert in Chile and controlled from the European Centre for Space Applications and Telecommunications (ECSAT) in Harwell, UK (Fig. 4). Future field test on Martian analogues are planned to investigate the synergy between Ma_MISS and WISDOM.

For more than ten years the MARSIS (Orosei et al., 2015) and SHARAD (Seu et al., 2007) radar sounders have been investigating the Martian subsurface. They operate at low frequency (2–20 MHz) from the Mars Express and the Mars Global Surveyor and orbiter, respectively. They have revealed subsurface structures in the polar regions (Phillips et al., 2008) as well as in the equatorial regions (Morgan et al., 2013). They have demonstrated the ability of the electromagnetic sounding to investigate the subsurface of Mars. WISDOM will follow their lead, but operating from the surface at a higher frequency better suited to characterize the shallow subsurface of Oxia Planum.

Declaration of competing interest

The authors declare that they have no known competing financial interests or personal relationships that could have appeared to influence the work reported in this paper.

CRediT authorship contribution statement

Y. Hervé: Writing - original draft, Conceptualization, Investigation, Software, Formal analysis. **V. Ciarletti:** Conceptualization, Writing - review & editing, Supervision, Funding acquisition, Investigation. **A. Le Gall:** Conceptualization, Writing - review & editing, Investigation. **C. Corbel:** Writing - review & editing, Project administration, Investigation. **R. Hassen-Khodja:** Writing - review & editing, Investigation. **W.S. Benedix:** Writing - review & editing, Investigation. **D. Plettemeier:** Conceptualization, Investigation. **O. Humeau:** Software, Investigation. **A.J. Vieau:** Project administration, Software, Investigation. **B. Lustrement:** Investigation. **S. Abbaki:** Investigation. **E. Bertran:** Software. **L. Lapauw:** Conceptualization. **V. Tranier:** Software, Investigation. **N. Oudart:** Formal analysis. **F. Vivat:** Software. **C. Statz:** Software. **Y. Lu:** Software. **S. Hegler:** Writing - review & editing. **A. Hérique:** Writing - review & editing.

Acknowledgement

Development of the WISDOM instrument and preparation of the data processing and interpretation have been funded and supported by CNES (Centre national d'études spatiales, France) and DLR (Deutsches Zentrum für Luft- und Raumfahrt, Germany).

Special thank for all the engineers, especially from LATMOS (Laboratoire Atmosphères, Milieux, Observations Spatiales, France), TUD (Technische Universität Dresden, Germany), and LAB (Laboratoire d'Astrophysique de Bordeaux, France) whose talents and hard work made the realization of WISDOM possible

Alice Le Gall is supported by Institut Universitaire de France (IUF). Nicolas Oudart is supported by CNES.

Appendix A. Supplementary data

Supplementary data to this article can be found online at https://doi.org/10.1016/j.pss.2020.104939.

References

Benedetto, Andrea, Tosti, Fabio, Ciampoli, Luca Bianchini, et al., 2017. An overview of ground-penetrating radar signal processing techniques for road inspections. Signal Process. 132, 201–209.

Benedix, W., Plettemeier, D., Zanoni, A., Preller, F., Ciarletti, V., 2013. Advance of WISDOM GPR antenna for ExoMars 2018 mission. In: IEEE International Conference on Wireless for Space and Extreme Environments, pp. 1–3. https://doi.org/10.1109/WiSEE.2013.6737553. Baltimore, MD.

Ciarletti, V., Corbel, C., Plettemeier, D., Cais, P., Clifford, S.M., Hamran, S., 2011. WISDOM GPR designed for shallow and high-resolution sounding of the martian subsurface. Proc. IEEE 99, 824–836.

Ciarletti, Valérie, Hervé, Yann, Dorizon, Sophie, Le Gall, Alice, Quantin, C., et al., 2015. Modelling the performances of the WISDOM radar on the Oxia Planum potential landing site for ExoMars. In: European Planetary Science Congress. Sep 2015, Nantes, France. pp.EPSC2015-E2574. insu-01211292.

Ciarletti, Valérie, Clifford, Stephen, Plettemeier, Dirk, Le Gall, Alice, Herve, Yann, et al., 2017. The WISDOM radar: unveiling the subsurface beneath the ExoMars rover and identifying the best locations for drilling. *Astrobiology*, Mary Ann Liebert 17 (6–7), 565–584. https://doi.org/10.1089/ast.2016.1532. https://hal-insu.archives-ouvertes.fr/insu-01575106.

Coates, A.J., Jaumann, R., Griffiths, A.D., Leff, C.E., Schmitz, N., Josset, J.-L., Paar, G., Gunn, M., Hauber, E., Cousins, C.R., Cross, R.E., Grindrod, P., Bridges, J.C., Balme, M., Gupta, S., Crawford, I.A., Irwin, P., Stabbins, R., Tirsch, D., Vago, J.L., Theodorou, T., Caballo-Perucha, M., Osinski, G.R., the PanCam Team, 2017. The PanCam instrument for the ExoMars rover. Astrobiology 17, 511–541.

Cook, J.C., 1975. Radar transparencies of mine and tunnel rocks. Geophysics 40, 865–885.

Cuomo, K.M., 4 Dec. 1992. A Bandwidth Extrapolation Technique for Improved Range Resolution of Coherent Radar Data, Project Report CJP-60, Revision 1. MIT Lincoln Laboratory.

De Sanctis, M.C., Altieri, F., Ammannito, E., Biondi, D., De Angelis, S., Meini, M., Mondello, G., Novi, S., Paolinetti, R., Soldani, M., Mugnuolo, R., Pirrotta, S., Vago, J.L., the Ma_Miss team, 2017. Ma_MISS on ExoMars: mineralogical characterization of the martian subsurface. Astrobiology 17, 612–620.

Dorizon, S., Ciarletti, V., Plettemeier, D., Benedix, W.S., 2015. Performances validation of the ExoMars 2018 WISDOM GPR in ice caves, Austria. Planet. Space Sci. 120, 1–14. https://doi.org/10.1016/j.pss.2015.10.008.

Friis, H.T., Crawford, A.B., Et Hogg, D.C., 1957. A reflection theory for propagation beyond the horizon. Bell System Technical Journal 36 (3), 627–644.

Garambois, Stéphane, Sénéchal, Pascale, , et al.Hervé, 2002. On the use of combined geophysical methods to assess water content and water conductivity of near-surface formations. J. Hydrol. 259 (1–4), 32–48.

Grimm, R.E., Heggy, E., Clifford, S., Dinwiddie, C., McGinnis, R., Farrell, D., 2006. Absorption and scattering in ground-penetrating radar: analysis of the Bishop Tuff. J Geophys Res Planets 111, E6. https://doi.org/10.1029/2005JE002619.

Gunes-Lasnet, et al., 2014. I-SAIRAS 2014. Canada, Montreal, 17–19 June 2014.

Hall, et al., 2019. In: In ASTRA 2019: 15th Symp. On Advanced Space Technologies in Robotics and Automation, vols. 27 – 28. Noordwijk, the Netherlands. May 2019.

Hervé, Yann, Ciarletti, Valerie, Corbel, Charlotte, Le Gall, Alice, Vieau, Andre-jean, Plettemeier, Dirk, Benedix, Wolf-Stefan, Oudart, Nicolas, 2019. Characterization and Performances of the WISDOM Ground Penetrating Radar for the ExoMars 2020 Mission, vol. 13. EPSC-DPS2019-1412-2.

Hervé, Yann, Ciarletti, Valérie, Le Gall, Alice, Corbel, Charlotte, Plettemeier, Dirk, et al., Jul 2019. WISDOM/ExoMars2020: A Calibrated and Fully Characterized Ground Penetrating Radar Ready to Sound the Martian Subsurface, Ninth International Conference on Mars. Pasadena, United States. pp.LPI Contribution No. 2089.

Huisman, Johan Alexander, Hubbard, Susan Sharpess, Redman, J. David, et al., 2003. Measuring soil water content with ground penetrating radar. Vadose Zone J. 2 (4), 476–491.

Josset, J.-L., Westall, F., Hofmann, B.A., Spray, J., Cockell, C., Kempe, S., Griffiths, A.D., De Sanctis, M.C., Colangeli, L., Koschny, D., Föllmi, K., Verrecchia, E., Diamond, L., Josset, M., Javaux, E.J., Esposito, F., Gunn, M., Souchon-Leitner, A.L., Bontognali, T.R.R., Korablev, O., Erkman, S., Paar, G., Ulamec, S., Foucher, F., Martin, P., Verhaeghe, A., Tanevski, M., Vago, J.L., 2017. The Close-Up Imager onboard the ESA ExoMars Rover: objectives, description, operations, and science validation activities. Astrobiology 17, 595–611.

Joudrier, et al., 2012. International Symposium on Artificial Intelligence, Robotics and Automation in Space (I-SAIRAS 2012), vols. 4–6, 2012.

Korablev, Oleg I., Dobrolensky, Yurii, Evdokimova, Nadezhda, et al., 2017. Infrared spectrometer for ExoMars: a mast-mounted instrument for the rover. Astrobiology 17 (6–7), 542–564.

Maser, K.R., Scullion, T., 1991. Automated pavement subsurface profiling using underground penetrating radar—case studies of four experimental field site. In: Transportation Research Board 70th Annual Meeting.

Mitrofanov, I.G., Litvak, M.L., Nikiforov, S.Y., Jun, I., Bobrovnitsky, Y.I., Golovin, D.V., Grebennikov, A.S., Fedosov, F.S., Kozyrev, A.S., Lisov, D.I., Malakhov, A.V., Mokrousov, M.I., Sanin, A.B., Shvetsov, V.N., Timoshenko, G.N., Tomilina, T.M., Tret'yakov, V.I., Vostrukhin, A.A., 2017. The ADRON-RM instrument onboard the ExoMars Rover. Astrobiology 17, 585–594.

Orosei, R., Jordan, R.L., Morgan, D.D., Cartacci, M., Cicchetti, A., Duru, F., et al., 2015. Mars advanced radar for subsurface and ionospheric sounding (MARSIS) after nine years of operation: a summary. Planet. Space Sci. 112, 98–114.

Oudart, Nicolas, Ciarletti, Valérie, Le Gall, Alice, Hervé, Yann, 2019. WISDOM/ExoMars: towards the High Resolution Imaging of the Martian Subsurface, vol. 13. EPSC-DPS2019-553-2.

Plettemeier, D., St Benedix, W., Statz, C., Lu, Y., Herve, Yann, et al., Sep 2017. Analysis methods for the polarimetric WISDOM radar aboard the ExoMars rover. In: European Planetary Science Congress 2017. Riga, Latvia. EPSC2017-E2870. insu-01664079.

Quantin-Nataf, C., Carter, J., Mandon, L., Balme, M., Fawdon, P., et al., 2019a. ExoMars at Oxia Planum, probing the aqueous-related noachian environments. In: Ninth International Conference on Mars. Lunar and Planetary Institute, Pasadena, United States. Jul 2019.

Quantin-Nataf, C., Carter, J., Mandon, L., Thollot, P., Loizeau, D., Pan, Lu, Dehouck, E., Millot, C., Breton, S., Bultel, Benjamin, Volat, M., Balme, M., Fawdon, P., Davis, Joel, Grindrod, Peter, Pacifici, Andrea, Gupta, S., Broyer, J., Allemand, Pascal, Ody, Anouck, Lozach, Loic, 2019b. Oxia Planum: the Selected Landing Site for the ExoMars 2020 Mission (submitted to Icarus).

Maria Carmela Raguso ; Marco Mastrogiuseppe ; Roberto Seu ; Lorenzo Piazzo, Super resolution and interferences suppression technique applied to SHARAD data 2018, 5th IEEE International Workshop on Metrology for AeroSpace (MetroAeroSpace) 10.1109/MetroAeroSpace.2018.8453529.

Saarenketo, Timo, Scullion, Tom, 2000. Road evaluation with ground penetrating radar. J. Appl. Geophys. 43 (2–4), 119–138.

Seu, R., Phillips, R.J., Biccari, D., Orosei, R., Masdea, A., Picardi, G., et al., 2007. SHARAD sounding radar on the Mars reconnaissance orbiter. J. Geophys. Res.: Plan 112 (E5).

Ulaby, F.T., Long, D.G., Blackwell, W.J., Elachi, C., Fung, A.K., Ruf, C., et al., 2014. Microwave Radar and Radiometric Remote Sensing, vol. 4. University of Michigan Press, Ann Arbor, p. 6.

Vago, Jorge L., Westall, Frances, Coates, Andrew J., Jaumann, Ralf, Korablev, Oleg, et al., 2017. Habitability on early Mars and the search for biosignatures with the ExoMars rover. *Astrobiology*, Mary Ann Liebert 17 (6–7), 471–510. https://doi.org/10.1089/ast.2016.1533.